Physique Numérique - Exercice 6

Study of the Quantum Harmonic Oscillator and the Tunnel Effect in a Potential Barrier

Jakob Adomeit, Nils Coutant
jakob.adomeit@epfl.ch, nils.coutant@epfl.ch

2nd August 2025

Table of contents

1 Introduction

This study examines the movement of a quantum mechanical particle in a potential governed by the Schrödinger equation. The equation is resolved numerically using the Crank-Nicolson scheme. Firstly, the quantum harmonic oscillator will be studied. For this simple case, the quantum evolution of the wave function will be compared to the classical trajectory of the particle. Further, the probability and average energy conservation as well as the conformity to the Heisenberg uncertainty principle will be verified. The convergence of the numerical simulation with respect to both the number of time steps and the number of spatial intervals will be verified. In the second part, the tunnel effect will be studied. The probability of transmission of the particle will be determined depending on the ratio between the energy of the particle and the size of the potential barrier. The probabilities of the particle being

on the left and on the right side of the potential barrier will be determined as functions of time and also compared to the classical case.

2 Theory

2.1 Statement of the problem

In the context of quantum mechanics, the movement of a particle of mass m in a unidimensional potential $V(x)$ is studied. The Hamiltonian of this system is

$$\hat{\mathcal{H}} = \frac{\hat{p}^2}{2m} + V(\hat{x}). \tag{1}$$

The potential, illustrated in figure 1, is given by

$$V(x) = \begin{cases} \frac{1}{2}m\omega_0^2 \left(\frac{x-x_a}{1-x_a/x_L}\right)^2 & \text{if } x \in [x_L, x_a] \\ V_0 \sin^2\left(\frac{\pi(x-x_a)}{x_b-x_a}\right) & \text{if } x \in [x_a, x_b] \\ \frac{1}{2}m\omega_0^2 \left(\frac{x-x_b}{1-x_b/x_R}\right)^2 & \text{if } x \in [x_b, x_R] \end{cases} \tag{2}$$

The particle is initially described as a Gaussian wave packet centered at $x = x_0$ and with standard deviation $\sigma = \sigma_{\text{norm}} L$ and wavenumber $k_0 = 2\pi n/L$:

$$\psi(x, t=0) = C \exp(ik_0 x) \exp\left[-(x-x_0)^2/(2\sigma^2)\right] \tag{3}$$

The constant C is chosen numerically such that the state is normalised, i. e. such that

$$\int_{x_L}^{x_R} |\psi(x,0)|^2 dx = 1 \tag{4}$$

The figure 2 illustrates the initial wavefunction $\psi(x, t=0)$.

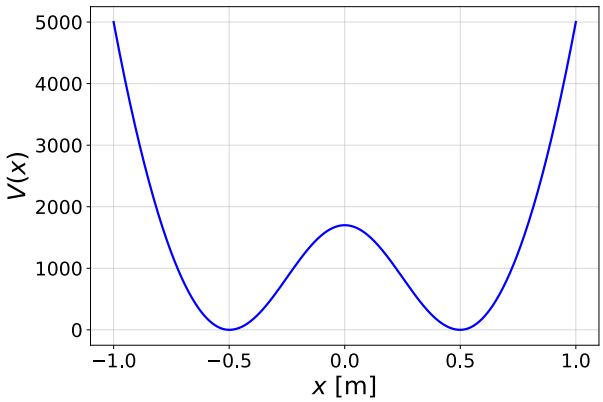

Figure 1: Graph of the potential $V(x)$ for $V_0 = 1300\,\text{J}$, $x_L = -1\,\text{m}$, $x_R = 1\,\text{m}$, $x_a = -0.5\,\text{m}$, $x_b = 0.5\,\text{m}$.

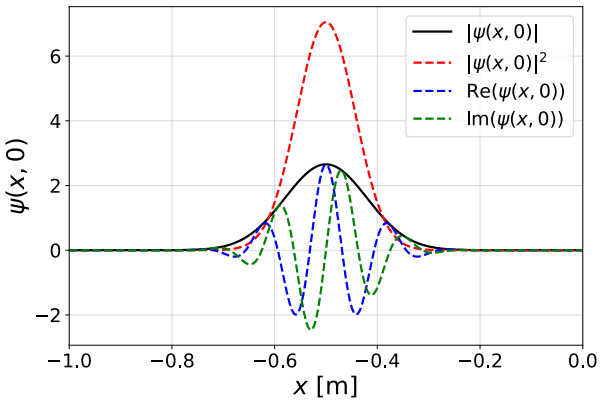

Figure 2: Graph of the initial wavefunction $\psi(x, t=0)$ for $\sigma_{\text{norm}} = 0.04\,\text{m}$, $n = 16$, $x_L = -1\,\text{m}$, $x_R = 1\,\text{m}$ and $x_0 = -0.5\,\text{m}$.

2.2 Analytical calculation of the classical harmonic oscillator

The Hamiltonian of the classical harmonic oscillator is given by

$$\mathcal{H}(x,p) = \frac{p^2}{2m} + V(x) = \frac{p^2}{2m} + \frac{1}{2}m\omega_0^2 x^2 \tag{5}$$

From the Hamiltonian formalism it follows that

$$\dot{x} = \frac{\partial \mathcal{H}}{\partial p} = \frac{p}{m}, \qquad \dot{p} = -\frac{\partial \mathcal{H}}{\partial x} = -m\omega_0^2 x \qquad \implies \ddot{x} = -\omega_0^2 x \tag{6}$$

Solving this system of differential equations gives

$$\begin{cases} x_{\text{class}}(t) = A\cos(\omega_0 t) + B\sin(\omega_0 t) \\ p_{\text{class}}(t) = -Am\omega_0 \sin(\omega_0 t) + Bm\omega_0 \cos(\omega_0 t) \end{cases} \tag{7}$$

Using the initial conditions $x(t=0) = x_0$, $p(t=0) = p_0$ to determine the constants A and B leads to

$$A = x_0, \qquad B = \frac{p_0}{m\omega_0}, \tag{8}$$

thus the classical position and momentum are given by

$$\begin{cases} x_{\text{class}}(t) = x_0\cos(\omega_0 t) + \frac{p_0}{m\omega_0}\sin(\omega_0 t) \\ p_{\text{class}}(t) = -x_0 m\omega_0 \sin(\omega_0 t) + p_0\cos(\omega_0 t). \end{cases} \tag{9}$$

2.3 Discretisation of the problem

The problem is discretised using n_{steps} time steps and n_x spacial intervals. Because the Hamiltonian is time-independent, the time evolution of the system is given by

$$\psi(x, t+\Delta t) = \exp\left(-\frac{i\Delta t}{\hbar}\mathcal{H}\right)\psi(x,t). \tag{10}$$

$$\implies \exp\left(\frac{i\Delta t}{2\hbar}\mathcal{H}\right)\psi(x,t+\Delta t) = \exp\left(-\frac{i\Delta t}{2\hbar}\mathcal{H}\right)\psi(x,t) \tag{11}$$

Approximating the exponential function by a first order Taylor series expansion gives

$$\left(1 + \frac{i\Delta t}{2\hbar}\mathcal{H}\right)\psi(x,t+\Delta t) = \left(1 - \frac{i\Delta t}{2\hbar}\mathcal{H}\right)\psi(x,t) \tag{12}$$

In its discretised form, $\psi(x,t)$ is represented by a vector, thus $\mathcal{H}$ is represented by a matrix with dimensions $n_x \times n_x$. At a fixed time t,

$$\mathcal{H}\psi_i = -\frac{\hbar^2}{2m}\cdot\frac{\psi_{i-1} - 2\psi_i + \psi_{i+1}}{(\Delta x)^2} + V_i \tag{13}$$

$$\implies \mathcal{H} = -\frac{\hbar^2}{2m(\Delta x)^2}\begin{pmatrix} -2 & 1 & & 0 \\ 1 & -2 & \ddots & \\ & \ddots & \ddots & 1 \\ 0 & & 1 & -2 \end{pmatrix} + \begin{pmatrix} V_1 & & & 0 \\ & V_2 & & \\ & & \ddots & \\ 0 & & & V_{n_x} \end{pmatrix} \tag{14}$$

In equation 12, one identifies the matrices $A = \left(1 + \frac{i\Delta t}{2\hbar}\mathcal{H}\right)$ and $B = \left(1 - \frac{i\Delta t}{2\hbar}\mathcal{H}\right)$. It is noted that $\mathcal{H}$, A and B are tridiagonal matrices, allowing for the system $A\psi(t+\Delta t) = B\psi(t)$ to be rather easily resolved numerically.
For the calculation of integrals, the trapeze rule is used [1]:

$$\int_a^b f(x)dx = \Delta x \sum_{i=1}^{N} \frac{f(x_i) + f(x_{i+1})}{2} + \mathcal{O}((\Delta x)^2) \tag{15}$$

where Δx is the size of the spatial intervals. At every time step, the simulation calculates the expectation values $\langle x \rangle$, $\langle x^2 \rangle$, $\langle p \rangle$, $\langle p^2 \rangle$ and $E = \langle \mathcal{H} \rangle$. The following is the calculation of $\langle p \rangle$, the other cases follow by analogy.

$$\langle p \rangle(t) = \int_{x_L}^{x_R} \psi^*(x,t) \left(-i\hbar \frac{\partial \psi(x,t)}{\partial x} \right) dx = -\frac{i\hbar}{2} \Delta x \sum_{i=1}^{n_x} \left(\psi^*(x_i,t) \frac{\partial \psi(x_i,t)}{\partial x} + \psi^*(x_{i+1}) \frac{\partial \psi(x_{i+1},t)}{\partial x} \right) \tag{16}$$

The partial derivatives of ψ are calculated using forward and backward finite differences on the left and right boundary respectively, and centered finite differences for the interior points. For the calculation of $E = \langle \mathcal{H} \rangle = \int_{x_L}^{x_R} \psi^*(x,t) \mathcal{H} \psi(x,t)$, a matrix multiplication is effectuated to compute $\mathcal{H}\psi(x,t)$. For the second partial derivatives of ψ in the calculation of $\langle p^2 \rangle$, centered finite differences are used for the interior points, while at the boundary points the second partial derivative is set to zero.

3 Harmonic Oscillator

In this first section, the Quantum Harmonic Oscillator is studied. This is done by taking the potential as $V(x) = \frac{1}{2} m \omega_0^2 x^2$, which corresponds to choosing $x_L = -1\,\text{m}$, $x_R = 1\,\text{m}$, $V_0 = 0\,\text{J}$ and $x_a = 0\,\text{m} = x_b$. Further, the initial wave packet is taken with $\omega_0 = 100\,\text{Hz}$, $x_0 = -0.5\,\text{m}$, $\sigma_{\text{norm}} = 0.04\,\text{m}$ and $n = 16$. The system is simulated up to $t_{\text{fin}} = 0.08\,\text{s}$.

3.1 Quantum motion and comparison with classical motion

A simulation is done with $n_x = 512$, $n_{\text{steps}} = 800$. The figure 3 illustrates the evolution of the modulus and the real part of $\psi(x,t)$. The results can also be found in form of an animation under this link.

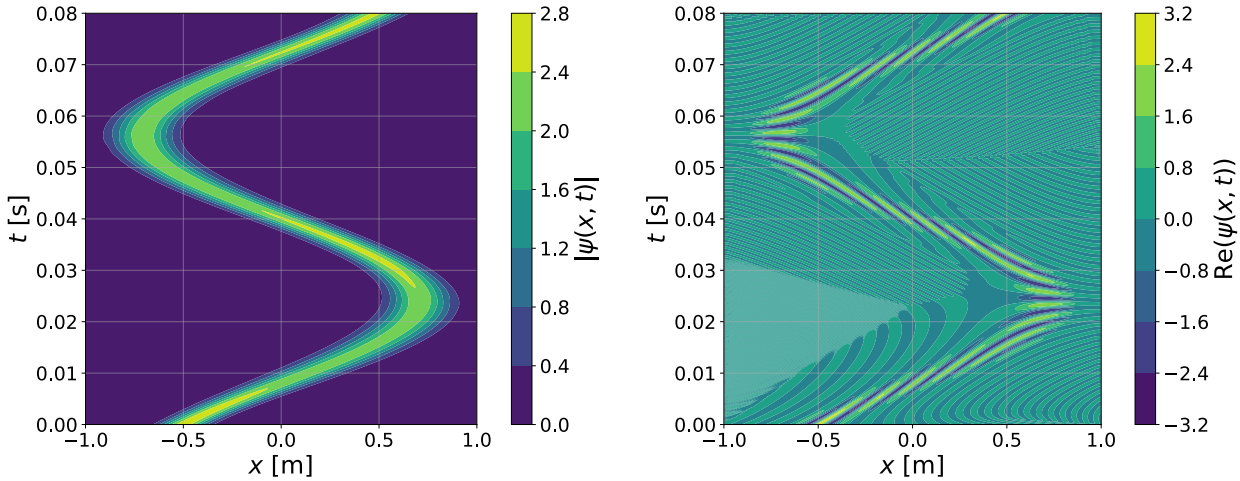

Figure 3: Evolution of the wave packet (a) $|\psi(x,t)|$ (b) $\text{Re}(\psi(x,t))$

It is observed that $|\psi(x,t)|$ retains its form of a Gaussian-envelope wave packet throughout the simulation. The figure 3b shows that the group velocity of the wave packet is greater than the phase velocity. Effectively, the individual wave crests in 3b have a greater gradient

than the envelope in 3, indicating an inferior velocity. This corresponds to the theoretical result that the group velocity, representing the particle's velocity, is twice the phase velocity. The figures 4 and 5 illustrates the average position $\langle x \rangle(t)$ and momentum $\langle p \rangle(t)$ in comparison with the movement of a classical particle determined in section 2.2.

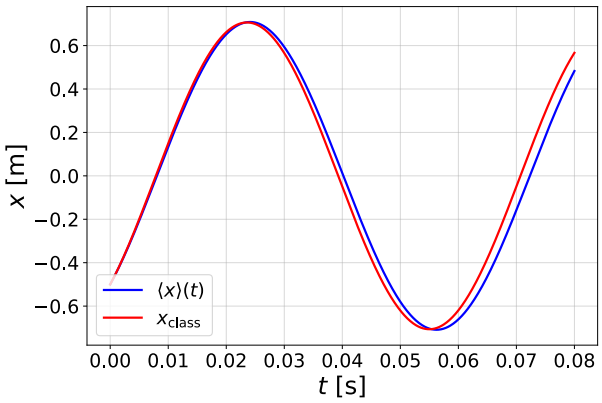

Figure 4: Comparison between $\langle x \rangle(t)$ and $x_{\text{class}}(t)$

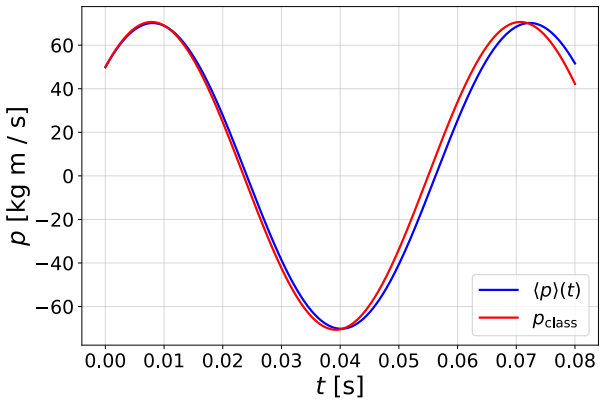

Figure 5: Comparison between $\langle p \rangle(t)$ and $p_{\text{class}}(t)$

For both position and momentum, an offset between the quantum mechanical expectation value and the classical quantity is observed. However, this offset is the result of truncation errors during the simulation rather than an inherent difference between the classical and the quantum mechanical case. This is illustrated by figure 6, which shows that for larger values of n_{steps} and n_x, the difference between the two graphs is much smaller compared to figure 4. The convergence of the simulation is further analysed in section 3.3.

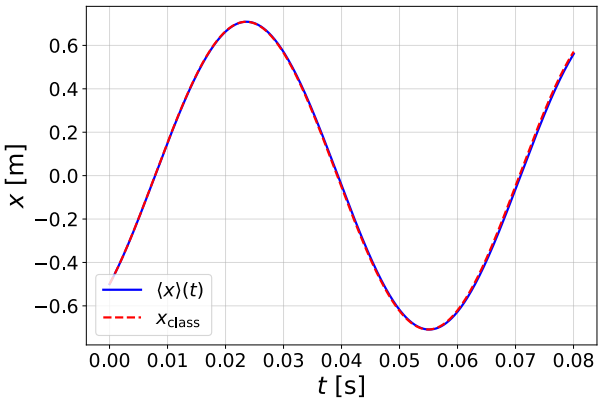

Figure 6: Comparison between $\langle x \rangle(t)$ and $x_{\text{class}}(t)$ for $n_{\text{steps}} = 2000$, $n_x = 2048$

3.2 Verification of physical properties

The probability of the particle being found in between the points $x = a$ and $x = b$ is given by

$$P_{a<x<b}(t) = \int_a^b |\psi(x,t)|^2 dx \tag{17}$$

Firstly, the conservation of total probability is evaluated. The figures 7 and 8 show the evolution of the total probability as well as the probability of the particle being in the left and right half respectively.

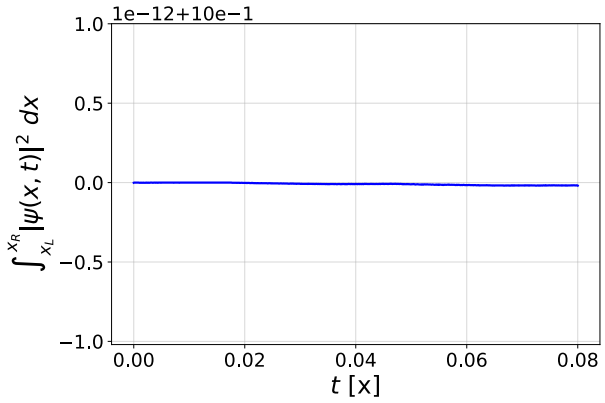

Figure 7: Evolution of the total probability $\int_{x_L}^{x_R} |\psi(x,t)|^2 dx$

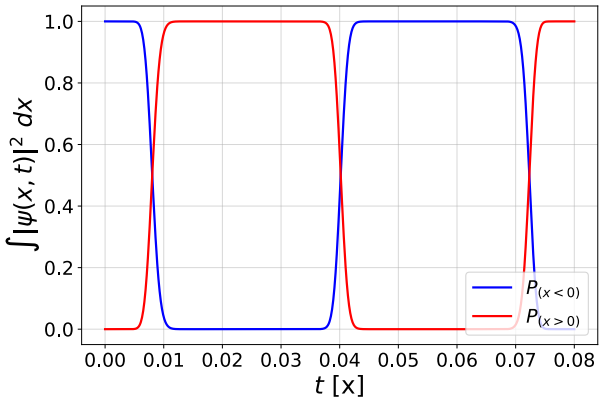

Figure 8: Evolution of probability of the particle being in the left and right half respectively

As expected, the total probability is conserved and equal to 1 throughout the simulation. Further, in figure 8 it can be seen clearly when the wavefunction passes from one side to the other. Similarly, figure 9 shows that the total energy is conserved as well.
The Heisenberg uncertainty principle reads

$$\Delta x \cdot \Delta p \geq \frac{\hbar}{2} \tag{18}$$

where ΔA is the standard deviation of the operator $\hat{A}$ which can be found as follows :

$$\Delta A = \sqrt{\langle \Delta \hat{A}^2 \rangle} = \sqrt{\langle \hat{A}^2 \rangle - \langle \hat{A} \rangle^2} \tag{19}$$

In figure 10 the evolution of $\Delta x \cdot \Delta p$ is illustrated. The graph confirms that the Heisenberg uncertainty is fulfilled during the simulation. Further, the graph reveals that at $t \simeq 0.06\,\mathrm{s}$, the quantity $\Delta x \cdot \Delta p$ is nearly minimised.

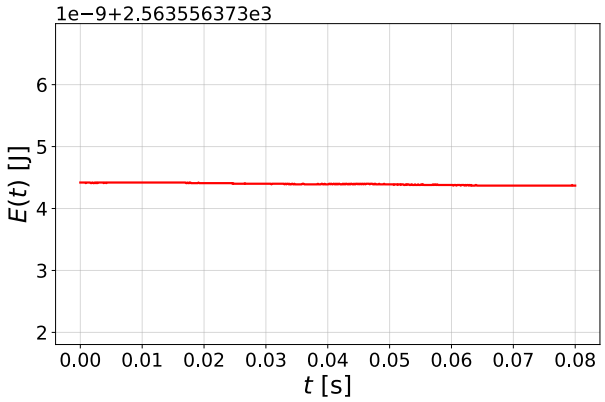

Figure 9: Time evolution of the energy $E(t) = \langle \mathcal{H} \rangle(t)$

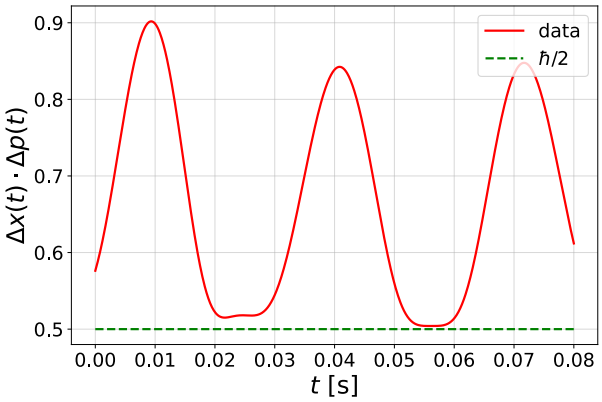

Figure 10: Verification of the Heisenberg uncertainty principle

3.3 Numerical convergence

In figure 11, the convergence graphs of $\langle x \rangle(t_{\mathrm{fin}})$ with respect to the number of time intervals n_{steps} as well as the number of spacial intervals n_x are shown. For comparison, the position of the classical harmonic oscillator at $t = t_{\mathrm{fin}}$, found in section 2.2, is also shown.

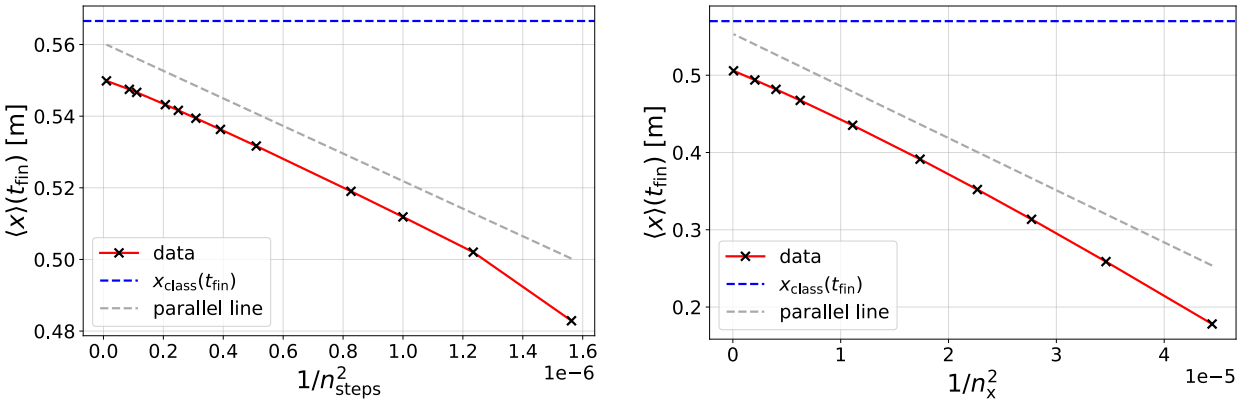

Figure 11: Convergence of $\langle x \rangle(t_{\text{fin}})$ with respect to (a) n_{steps} (b) n_x

The graphs lead to the conclusion that $\langle x \rangle(t_{\text{fin}})$ converges of order 2 with respect to both n_{steps} and n_x. At first, it appears from 11 that $\langle x \rangle(t_{\text{fin}})$ does not converge towards the analytical result for the position of the classical harmonic oscillator. However, this results from the fact that the convergence is examined with respect to n_{steps} and n_x separately. Effectively, both parameters introduce errors and limit the accuracy of the simulation. Thus, another convergence analysis was effectuated by setting $n_{\text{steps}} = n_{\text{steps},0} \cdot n_{\text{mult}}$ and $n_x = n_{x,0} \cdot n_{\text{mult}}$ and varying n_{mult}. The results in figure 12 show that $\langle x \rangle(t_{\text{fin}}) \to x_{\text{class}}$ when $1/n_{\text{steps}}, 1/n_x \to 0$. Thus, the convergence is of second order with respect to n_{mult}. However, the effectuated numerical calculations scale proportionally to $n_x \cdot n_{\text{steps}}$. Given that $n_x \cdot n_{\text{steps}} \propto n_{\text{mult}}^2$, it is concluded that the overall convergence of $\langle x \rangle(t_{\text{fin}})$ is of first order with respect to $n_x \cdot n_{\text{steps}}$.

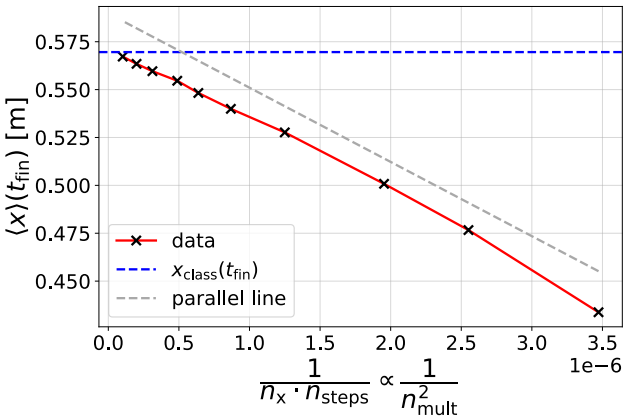

Figure 12: Convergence of $\langle x \rangle(t_{\text{fin}})$ with respect to n_{steps} and n_x simultaneously

4 Potential Barrier and Tunnel Effect

4.1 Transmission probability analysis

The parameters of the potential defined by the equation (2) are now set to $V_0 \neq 0$, $x_a = -0.5$ m, $x_b = 0.5$ m and the initial wave function is kept the same. The effect of the potential barrier on the probabilities of finding the particle on the left side $P_{(x<0)}$ or on the right side $P_{(x>0)}$ of the barrier will be studied. At the time $t_{\text{trans}} = 0.035$ s, the particle is considered to have entirely bounced off or crossed the obstacle. The figure 13 represents the probability $P_{\text{trans}} = P_{(x>0)}(t_{\text{trans}})$ that the particle has gone through the barrier as a function of V_0 and as a function of $\langle E \rangle / V_0$. As shown in the section 3.2, the average $\langle E \rangle$ is conserved during each simulation, so it can be taken as the energy average at time $t = 0$ s.

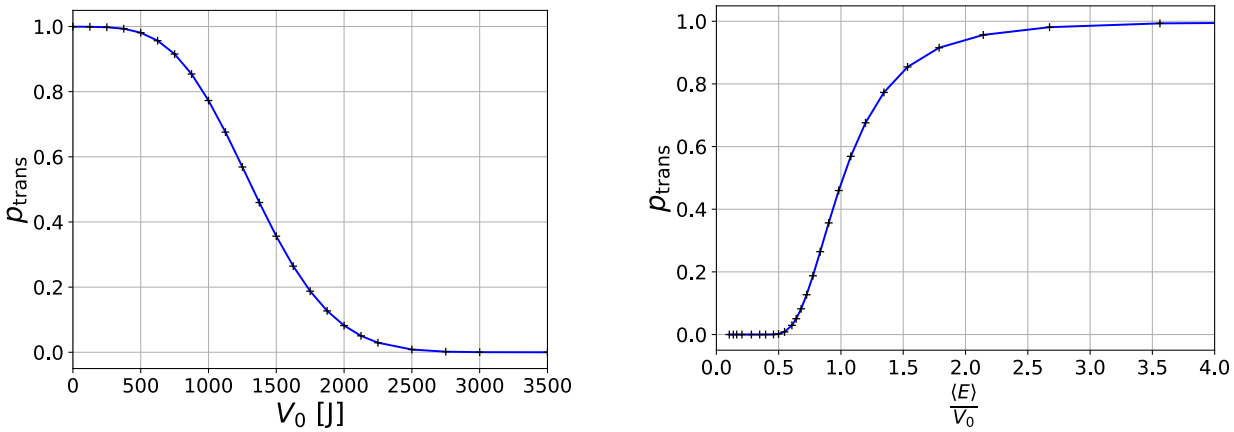

Figure 13: Probability P_{trans} of finding the particle on the right side of the barrier at time t_{trans} (a) as a function of V_0 (b) depending on $\langle E \rangle / V_0$

As expected, the probability of transmission p_{trans} decreases as V_0 increases. First, the average of the energy $\langle E \rangle$ varies slightly with V_0, but it can generally be considered to be around $\langle E \rangle \simeq 1300$ J. While below $V_0 < 500$ J, the particle is almost entirely transmitted, it is observed that for larger values, the probability p_{trans} decreases even though the energy $\langle E \rangle > V_0$ is sufficient for the particle to cross the barrier in the classical case. p_{trans} seems to be around 1/2 at $V_0 \simeq \langle E \rangle$. For $V_0 > \langle E \rangle$, the classical particle wouldn't be able to cross the barrier, but the probability of transmission p_{trans} is not zero. The probability p_{trans} is close to zero for $V_0 \simeq 2600$ J, which can be linked with $2\langle E \rangle$. The second graph confirms these observations. In fact, with $\langle E \rangle / V_0 = 1/2$, p_{trans} is close to zero, for $\langle E \rangle / V_0 \simeq 1$, it is close to 1/2 and for $\langle E \rangle / V_0 > 2$, the probability p_{trans} approaches 1.

4.2 Evolution of the wave function $\psi(x, t)$

The aim is now to gain a better understanding of how the wave function $\psi(x, t)$ interacts with the potential barrier. Four cases will be studied: $V_0 = 500\,\text{J} < \langle E \rangle$, $V_0 = 1300\,\text{J} \simeq \langle E \rangle$, $V_0 = 1700\,\text{J} > \langle E \rangle$ and $V_0 = 2500\,\text{J} \gg \langle E \rangle$. The figure 14 shows the distribution of the wave function modulus evolving with t for these four simulations. These linked animations can also help visualize how the particle progress for $V_0 < \langle E \rangle$, $V_0 \simeq \langle E \rangle$, $V_0 > \langle E \rangle$ and $V_0 \gg \langle E \rangle$. The simulations are effectuated up to $t_{\text{end}} = 0.08\,\text{s}$.

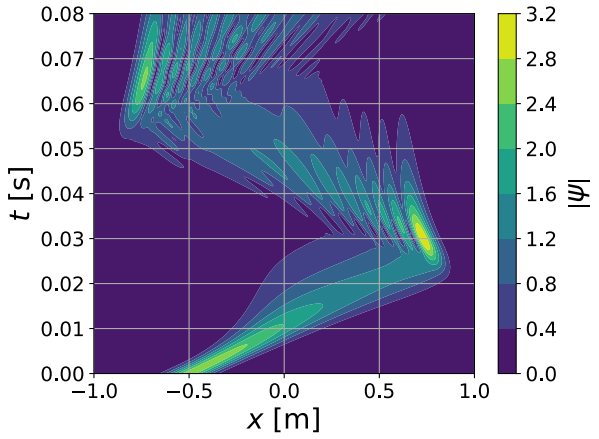

(a) $V_0 = 500$ J $< \langle E \rangle$

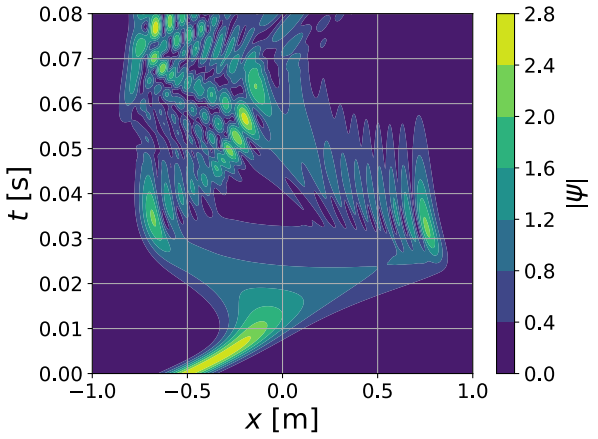

(b) $V_0 = 1300$ J $\simeq \langle E \rangle$

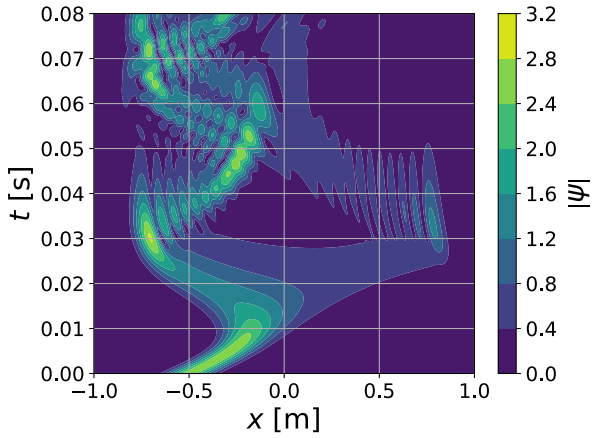

(c) $V_0 = 1700$ J $> \langle E \rangle$

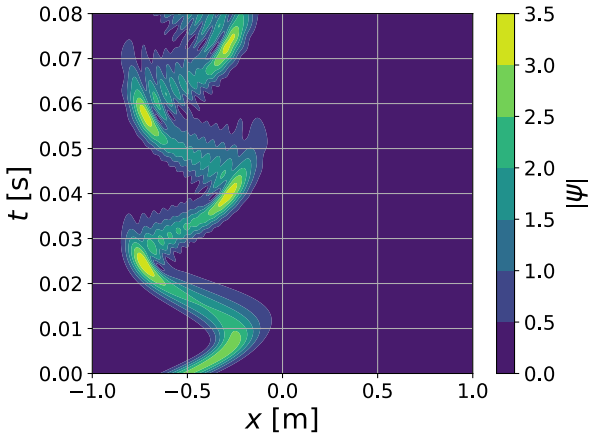

(d) $V_0 = 2500$ J $\gg \langle E \rangle$

Figure 14: Evolution of the wave function modulus $|\psi(x,t)|$ for different potential heights V_0

As seen before, for $V_0 = 500$ J $< \langle E \rangle$ the particle is almost entirely transmitted. But the dispersion of the wave function is now also visible on the graph and on the animation. This effect is caused by the short wavelength travelling faster than the longer ones. For $V_0 = 1300$ J $\simeq \langle E \rangle$, the wave function splits into almost two equally distributed packets. The two packets each interfere with themselves when they bounce against the end of the potential. When they reach the potential barrier a second time, the reflected part of the left packet, and the transmitted part of the right packet create an interference pattern. It is possible to observe minima and maxima of the wave function modulus $|\psi(x,t)|$ on the left side of the barrier. Furthermore, the animation shows that the shorter wavelengths appear to penetrate the potential barrier more easily. Effectively, these radiations hold more energy. For $V_0 = 1700$ J $> \langle E \rangle$, as observed before, the transmission probability is non-zero but significantly reduced compared to previous cases. Also, the wavelengths that were able to cross are the shorter ones. Finally, for $V_0 = 2500$ J $\gg \langle E \rangle$ the particle is almost entirely reflected.

The figure 15 represents the probabilities of finding the particle on the left side of the potential barrier $P_{(x<0)}$ and on the right side of it $P_{(x>0)}$ as a function of time with an offset

of $\tau = 0.0257$ s and depending on V_0. The simulation has been extended to a duration of $t_{\text{end},2} = 3t_{\text{end}} = 0.24$ s to analyse how the probabilities evolve after a long time. These probabilities are also compared with the classical ones given by

$$P^{\text{class}}_{(x<0)}(t) = \begin{cases} 1 & \text{if } E < V_0 \\ 1 & \text{if } E \geq V_0 \text{ et } t \bmod T < T/2 \\ 0 & \text{otherwise} \end{cases} \qquad P^{\text{class}}_{(x>0)}(t) = 1 - P_{(x<0)}(t)$$

with T the classical period, calculated numerically for $E = \langle E \rangle > V_0$ with this integral

$$T = 2 \cdot \int_{-\delta}^{\delta} \frac{dx}{v(x)} = \sqrt{2m} \cdot \int_{-\delta}^{\delta} \frac{1}{\sqrt{E - V(x)}} \mathrm{d}x$$

$\pm\delta$ are the boundaries of the position that the classical particle can reach, defined by $V(\pm\delta) = E$. For $V_0 = 500$ J, the classical period is $T_{500} = 0.07490$ s which is larger than $\frac{2\pi}{\omega_0}$. For $V_0 = E$, the classical particle takes an infinitely long time to reach the top of the barrier.

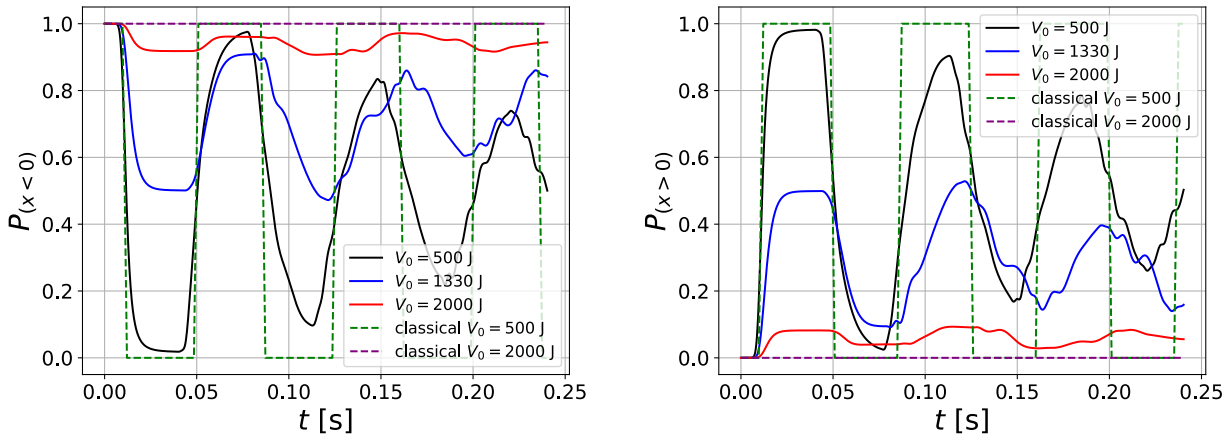

Figure 15: Probabilities of finding the particle on both sides of the potential barrier as a function of time t for four values of V_0 (a) Left side $P_{(x<0)}(t)$ (b) Right side $P_{(x>0)}(t)$

For $V_0 = 500$ J $< \langle E \rangle$, the probabilities of the first pattern are close to the classical ones. The classical period T_{500} also seems to match the simulation. For the following patterns, the probabilities tend to balance, reach 1/2, and they deviate from the classical predictions. By increasing V_0, $P_{(x<0)}$ also increases and the probabilities are further away from the classical ones. For $V_0 = 1300$ J $\simeq \langle E \rangle$, this effect is indeed visible. The observed period T is longer but not infinite like the classical one. For $V_0 = 2000$ J $> \langle E \rangle$, the probabilities continue to oscillate and they are also close to the classical probabilities. By increasing even more V_0, $P_{(x<0)}$ would approach the classical probability which is 1.

5 Optional

5.1 Detection of the particle

A particle detector was implemented for the right half of the system. If activated, at time $t = t_{\text{detect}}$, the wavefunction is multiplied by a function $f(x)$ and subsequently renormalised, where

$$f(x) = \begin{cases} 0 & x < 0 \\ \sin^2\left(\frac{\pi x}{2x_{da}}\right) & 0 \le x < x_{da} \\ 1 & x_{da} \le x < x_{db} \\ \cos^2\left(\frac{\pi(x-x_{db})}{2(x_R-x_{db})}\right) & x_{db} \le x \le x_R \end{cases} \tag{20}$$

The constants were chosen $x_{da} = 0.2$ and $x_{db} = 0.8$ and the simulation from section 4 of a potential barrier with $V_0 = 1700\,\mathrm{J}$ was repeated, but with a detection at $t_{\text{detect}} = 0.04\,\mathrm{s}$. The figure 16 and this animation illustrate the evolution of the wavefunction. For comparison, the evolution without detection is shown in figure 14. At the instant of detection, the part of the wavefunction which was reflected disappears, and due to the renormalisation the part that has been transmitted increases in amplitude.

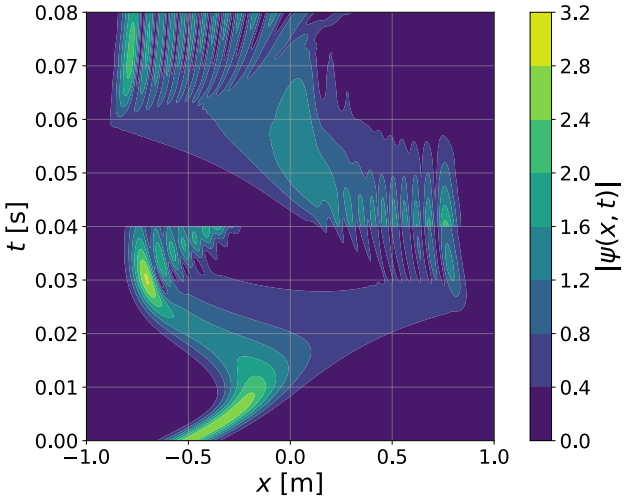

Figure 16: Evolution of the wavefunction with a potential barrier with $V_0 = 1700\,\mathrm{J}$ and a detection in the right half at $t_{\text{detect}} = 0.04\,\mathrm{s}$

5.2 Periodic potential

The potential

$$V(x) = V_0 \sin\left(n_{\text{pot}} \frac{2\pi x}{L}\right)$$

serves as an approximation of the energy landscape in a crystal, as explained in the course notes [2]. The parameters are set to $V_0 = 500\,\mathrm{J}$, $n_{\text{pot}} = 40$, and $L = 4\,\mathrm{m}$. The initial wavefunction is defined by equation (3) with the values $n = 20$, $x_0 = -0.5\,\mathrm{m}$, and $\sigma_{\text{norm}} = 0.04\,\mathrm{m}$.
For a specific energy level, the expectation value of the momentum is zero, and the particle remains stationary, as illustrated in Figure 17 and the accompanying video. These results have important applications in solid-state physics.

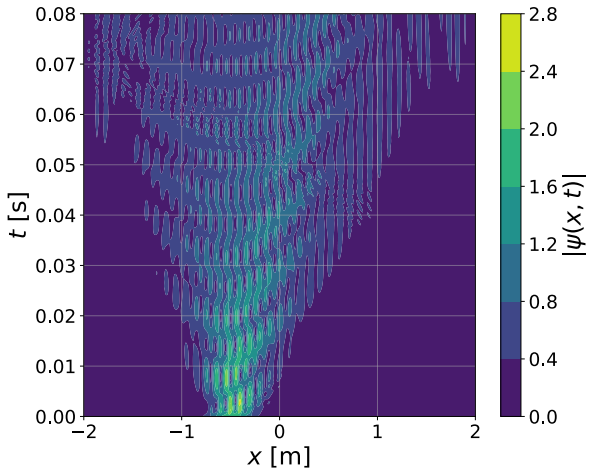

Figure 17: Evolution of the wavefunction with a sinusoidal potential

6 Conclusion

The study explored the quantum harmonic oscillator and the tunneling effect through a potential barrier by numerically solving the time-dependent Schrödinger equation using the Crank–Nicolson scheme. In the first part, the quantum harmonic oscillator was examined

through a comparison between the quantum evolution of the wave function and the classical trajectory of a particle. The modulus and real part of the wave function were visualized, and the quantum expectations $\langle x \rangle(t)$ and $\langle p \rangle(t)$ were compared with their classical counterparts $x_{\text{class}}(t)$ and $p_{\text{class}}(t)$. The conservation of total probability and average energy, as well as the validity of Heisenberg's uncertainty principle, were then verified. Numerical convergence of the final average position was studied and was found to be of second order with respect to both the number of time steps and the number of spatial intervals individually. However, it was found that the overall convergence of $\langle x \rangle(t_{\text{fin}})$ is of first order with respect to $n_x \cdot n_{\text{steps}}$. In the second part, a potential barrier was introduced to investigate the quantum tunneling effect. The transmission probability was analysed as a function of both the particle's average energy and the barrier height. The evolution of the wave function was illustrated for representative scenarios. Additionally, the time-dependent probabilities of finding the particle on either side of the barrier were compared with classical expectations. Finally, a particle detector was simulated to analyze how the wave function evolves when the particle is detected on the right side of the barrier.
By providing clear visual representations of the system's evolution, the study contributed to a more intuitive understanding of key quantum phenomena such as wave packet spreading, self-interference, and quantum tunneling.

References

[1] Laurent Villard. Physique numérique - epfl - notes du cours phys-210, 2025. URL: https://moodle.epfl.ch/course/view.php?id=287.

[2] EPFL. Physics numerics week 14 lecture slides. https://moodle.epfl.ch/pluginfile.php/77921/mod_resource/content/297/Presentations/PhysNum25Week14.pdf, 2025. Accessed on 2025-05-28.

[3] Laurent Villard et Dr Giovanni Di Giannatale. Physique numérique lv spc epf - physique numérique – exercice 6 Énoncé, 2025. URL: https://moodle.epfl.ch/pluginfile.php/77641/mod_resource/content/30/Exercice6_2025.pdf.

Appendices

Values used in the simulations

Parameter	Value
t_{fin} [s]	0.08
x_L [m]	-1
x_R [m]	1
x_a [m]	0
x_b [m]	0
ω_0 [Hz]	100
V_0 [J]	0
x_0 [m]	-0.5
σ_{norm} [m]	0.04
n	16
n_{steps}	800
n_x	512

Table 1: Values of the parameters for the section 3 on the harmonic oscillator [3]

Parameter	Value
t_{end} [s]	0.08
x_L [m]	-1
x_R [m]	1
x_a [m]	-0.5
x_b [m]	0.5
ω_0 [Hz]	100
x_0 [m]	-0.5
σ_{norm} [m]	0.04
n	16
n_{steps}	800
$n_{\text{intervals}}$	512

Table 2: Values of the parameters for the section 4 on the tunnel effect [3]

Finite differences and Trapeze rule

First order centered:

$$f_i' = \frac{f_{i+1} - f_{i-1}}{2h_x}$$

First order forward:

$$f_i' = \frac{f_{i+1} - f_i}{h_x}$$

First order backward:

$$f_i' = \frac{f_i - f_{i-1}}{h_x}$$

Second order centered:

$$f_i'' = \frac{f_{i+1} - 2f_i + f_{i-1}}{h_x^2}$$

Trapeze rule:

$$\int_a^b f(x)dx = h\sum_{i=1}^{N} \frac{f(x_i) + f(x_{i+1})}{2} + \mathcal{O}(h^2)$$